


Engineering Floquet topological phases using elliptically polarized light

Ranjani Seshadri^{1,*} and Diptiman Sen^{2,†}

¹*Department of Physics, Ben-Gurion University of the Negev, Beer-Sheva 84105, Israel*

²*Centre for High Energy Physics, Indian Institute of Science, Bengaluru 560012, India*

 (Received 19 July 2022; revised 30 September 2022; accepted 17 November 2022; published 1 December 2022)

We study a two-dimensional topological system driven out of equilibrium by the application of elliptically polarized light. In particular, we analyze the Bernevig-Hughes-Zhang model when it is perturbed using an elliptically polarized light of frequency Ω described in general by a vector potential $\mathbf{A}(t) = (A_{0x} \cos(\Omega t), A_{0y} \cos(\Omega t + \phi_0))$. Even for a fixed value of ϕ_0 , we can change the topological character of the system by changing the x and y amplitudes of the drive. We therefore find a rich topological phase diagram as a function of A_{0x} , A_{0y} , and ϕ_0 . In each of these phases, the topological invariant given by the Chern number is consistent with the number of spin-polarized states present at the edges of a nanoribbon.

DOI: [10.1103/PhysRevB.106.245401](https://doi.org/10.1103/PhysRevB.106.245401)

Introduction. Topological insulators (TIs)—exotic phases of matter characterized by a gapped bulk hosting robust, conducting boundary modes—have been the talk of the town for the last several years [1–6]. A defining feature of such systems is the existence of a bulk-boundary correspondence; that is, a topological invariant (for example, a Chern number for two-dimensional TIs) derived from the bulk bands defines the properties of the boundary modes. While such topological systems are, by themselves, quite interesting to study, driving them out of equilibrium using an external perturbation periodic in time constitutes a rapidly evolving area of research [7–24]. In particular, one can generate topological phases by driving a system which was nontopological to begin with. The underlying reason for this is that while the instantaneous Hamiltonian lies in a trivial phase, the unitary time-evolution operator over one drive cycle is topological and has eigenstates localized near the boundaries. Such systems are studied using Floquet theory, which relies on perfect time periodicity of the drive, and are termed Floquet topological phases.

Irradiating materials with polarized light is one way of experimentally generating Floquet topological phases. Several studies have demonstrated that using circularly polarized light to drive materials can generate and/or modify topological phases [25–33]. However, to the best of our knowledge, there are relatively few works which have studied the effect of the more general case of elliptically polarized light [17,34–37]. While the effect of using elliptically polarized light may seem to be qualitatively similar to that of circularly polarized light in some aspects, some features are markedly different. The deviation from perfect circular polarization introduces an anisotropy into the time-dependent model, thereby significantly modifying the topological properties.

This paper addresses the effect of tweaking the polarization of light on the topological phase diagram of a

two-dimensional Floquet topological system—the Bernevig-Hughes-Zhang (BHZ) model—driven using an elliptically polarized light. Such a drive can in general be created by superposing two linear or circularly polarized beams having a phase difference. We find that the topological invariant associated with this driven system, namely, the Floquet Chern number, depends on the phase of the polarized light as well as on the relative amplitudes in the two directions.

Equilibrium model. The half-BHZ system [2] with mass M and spin-orbit coupling (SOC) Δ is governed by the Hamiltonian $H = \psi_{\mathbf{k}}^\dagger h(\mathbf{k}) \psi_{\mathbf{k}}$, where $\psi_{\mathbf{k}}$ is the spinor $(c_{\mathbf{k},\uparrow}, c_{\mathbf{k},\downarrow})^\dagger$ and

$$h(\mathbf{k}) = \mathbf{d}(\mathbf{k}) \cdot \boldsymbol{\sigma}, \quad (1)$$

with $\mathbf{d}(\mathbf{k}) = (\Delta \sin k_x, \Delta \sin k_y, M + \gamma \cos k_x + \gamma \cos k_y)$. Here, $\sigma^{x,y,z}$ are the 2×2 Pauli matrices, and γ is the nearest-neighbor tight-binding hopping amplitude, which we will generally set to unity (we will also set $\hbar = 1$). Two obvious symmetries of the Hamiltonian in Eq. (1) are the fourfold rotation $C_4 = \{e^{-i(\pi/4)\sigma^z} | (k_x, k_y) \rightarrow (k_y, -k_x)\}$ about the z axis, and the charge conjugation or particle-hole symmetry \mathcal{P} such that $\mathcal{P}h(\mathbf{k})\mathcal{P}^{-1} = -h^*(-\mathbf{k})$. Moreover, while the standard time-reversal symmetry Θ is absent, $h(\mathbf{k})$ has a modified time-reversal symmetry defined as $\mathcal{T}h(\mathbf{k})\mathcal{T}^{-1} = h(\mathbf{k})$, where $\mathcal{T} = \mathcal{M}_x\Theta$ and \mathcal{M}_x is a reflection about the $k_x = 0$ line. This system falls under class D in the Altland-Zirnbauer classification [38].

For a nonzero Δ , the spectrum is gapped, in general, except when $M = 0, \pm 2$. Calculating the Chern number C_+ for the top band using the method prescribed by Fukui *et al.* [39], we obtain the phase diagram at equilibrium, shown in Fig. 1(a), and see that

$$C_+ = \begin{cases} +1 & \text{for } -2 < M < 0 \\ -1 & \text{for } 0 < M < 2 \\ 0 & \text{for } |M| > 2. \end{cases} \quad (2)$$

According to the bulk-boundary correspondence an infinitely long nanoribbon running parallel to the x axis and having a

*ranjanis@post.bgu.ac.il

†diptiman@iisc.ac.in

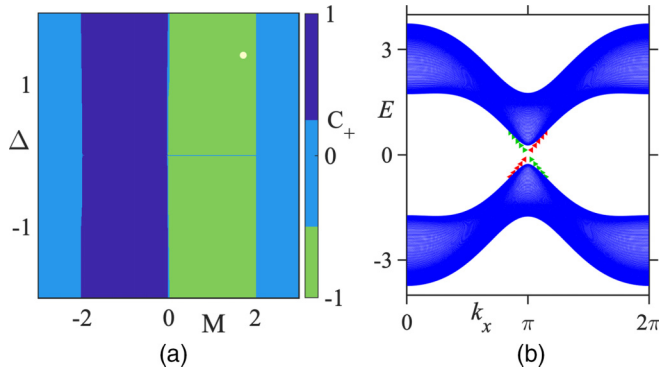


FIG. 1. (a) The phase diagram of a half-BHZ system with trivial and topological phases. (b) Edge state spectrum for a nanoribbon 100 sites wide. We have chosen $M = \sqrt{3}$ and $D = \sqrt{2}$ corresponding to the white dot in (a). The bulk states (blue) are gapped with the edge modes residing in the gap. The right-pointing (left-pointing) triangles denote spin pointing along the \hat{x} ($-\hat{x}$) directions, while the color red (green) corresponds to states localized at the bottom (top) edge of the ribbon.

finite width of N_y sites in the \hat{y} direction should have edge modes localized at the top and bottom edges with energies lying in the bulk gap. To verify this, we diagonalize the following one-dimensional Hamiltonian obtained by setting the good quantum number k_x as a parameter:

$$H_{k_x}^{\text{1D}} = h_{k_x} + \sum_{n_y} \frac{\gamma}{2} (c_{n_y, \uparrow}^\dagger c_{n_y+1, \uparrow} - c_{n, \downarrow}^\dagger c_{n_y+1, \downarrow}) - \sum_{n_y} \frac{\Delta}{2} (c_{n_y, \uparrow}^\dagger c_{n_y+1, \downarrow} - c_{n, \downarrow}^\dagger c_{n_y+1, \uparrow}), \quad (3)$$

where $h_{k_x} = \mathbb{I}_{N_y} \otimes ((M + \gamma \cos k_x) \sigma^z + \Delta \sin k_x \sigma^x)$ is a $2N_y \times 2N_y$ matrix containing the k_x -dependent terms. Figure 1(b) shows the bulk and edge-state spectrum obtained from Eq. (3). Edge states localized on the top and bottom edges (green and red, respectively) have energies in the gap between the bulk bands (shown in blue). These edge states are also eigenstates of σ^x with the right- and left-pointing triangles corresponding to $\sigma^x = 1$ and $\sigma^x = -1$, respectively. Clearly, all the right-moving modes with group velocity $v_g = \partial E / \partial k_x > 0$ are localized on the bottom edge and have $\sigma^x = -1$, whereas the left movers (i.e., $v_g < 0$) lie on the top edge and have $\sigma^x = 1$.

Floquet topological phases. We now introduce a time dependence into the problem by using a polarized light with a vector potential \mathbf{A} of the form

$$\mathbf{A}(t) = (A_{0x} \cos(\Omega t), A_{0y} \cos(\Omega t + \phi_0)), \quad (4)$$

where ϕ_0 is the phase difference between the x and y components. This is the most general form of \mathbf{A} associated with elliptically polarized light. The time-dependent electric field is therefore $\mathbf{E}(t) = -\partial \mathbf{A} / \partial t = (E_{0x} \sin(\Omega t), E_{0y} \sin(\Omega t + \phi_0))$, where $E_{0x(y)} = \Omega A_{0x(y)}$. The vector potential in Eq. (4) enters the momentum-space Hamiltonian via minimal coupling, $\mathbf{k} \rightarrow \mathbf{k} + \mathbf{A}$. Therefore the bulk Hamiltonian in Eq. (1) is modified as $h(\mathbf{k}) \rightarrow h(\mathbf{k} + \mathbf{A})$. We note that linear polarization and circular polarization are special cases of Eq. (4). When $\phi_0 = \pm\pi/2$, we obtain elliptically polarized

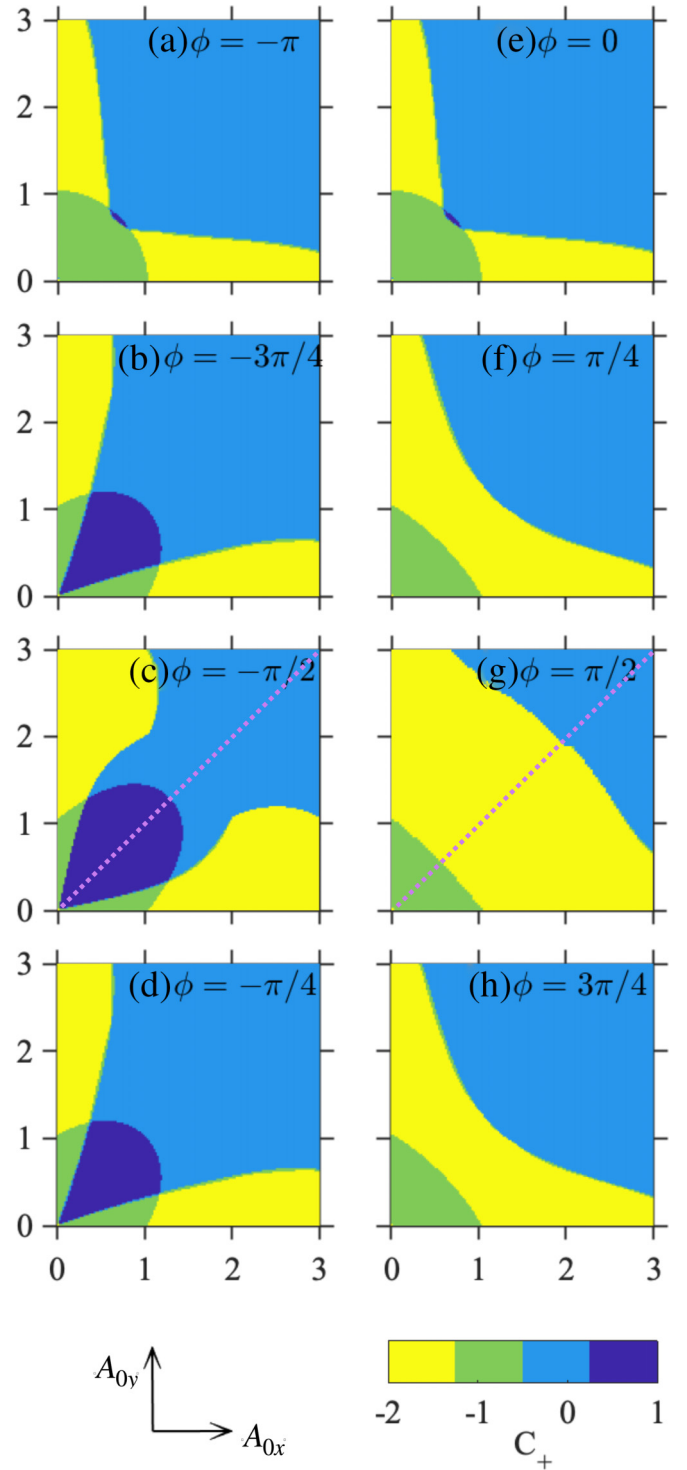


FIG. 2. (a)–(h) Floquet Chern number C_+ of the positive quasienergy band, as a function of drive amplitudes A_{0x} and A_{0y} , for different phases ϕ_0 of the elliptically polarized light. We set the equilibrium parameters $M = \sqrt{3}$ and $\Delta = \sqrt{2}$ corresponding to the white dot marked in Fig. 1(a). The $A_{0x} = A_{0y}$ line in (c) and (g) corresponds to circularly polarized light. We have used $\Omega = 5$, which is much higher than the band gap.

light with the axes of the ellipse aligned with the cardinal axes. Furthermore, if $A_{0x} = A_{0y}$ and $\phi_0 = \pm\pi/2$, we obtain

left- or right-circularly-polarized light. Since the drive is perfectly periodic, we employ Floquet theory and calculate the quasienergy eigenvalues and eigenvectors by diagonalizing the Floquet operator defined as the time-evolution operator over one cycle, i.e., $\mathcal{U}_T = \mathfrak{T} \exp(-i \int_0^T dt H(t))$,

$$\mathcal{U}_T \psi_\alpha = e^{-i\epsilon_\alpha T} \psi_\alpha. \quad (5)$$

The Floquet eigenvalues ϵ_α are unique modulo $n\Omega$, where n is an integer, with $n = 0$ corresponding to the primary Floquet zone. (See Supplemental Material [40] and Refs. [41,42].)

The Floquet eigenstates ψ_α are then used to calculate the Chern numbers. Figure 2 shows the rich topological phase diagram as a function of the drive amplitudes for different values of ϕ , for a fixed frequency $\Omega = 5$, which is much greater than the band gap.

We find that purely changing the ratio of the x and y amplitudes of the elliptically polarized light takes us from one phase to another which is topologically distinct. We have chosen the parameters ($M = \sqrt{3}$, $\Delta = \sqrt{2}$) such that in the absence of a drive we are in a topologically nontrivial phase with Chern number $C_+ = -1$. This is marked as a white dot in Fig. 1(a).

We note two symmetries in the plots in Fig. 2. First, for each value of ϕ_0 , the plots are symmetric about the $A_{0x} = A_{0y}$ line. Second, the plots for ϕ_0 and $\pi - \phi_0$ look identical. We can understand these two symmetries as follows. Given $h(k_x, k_y, A_{0x}, A_{0y}, \phi_0, t)$, the time-dependent periodic Hamiltonian with frequency Ω , the Floquet operator is given by

$$\mathcal{U}_T = \mathfrak{T} e^{-i \int_0^T dt h(k_x, k_y, A_{0x}, A_{0y}, \phi_0, t)}. \quad (6)$$

Noting that $\cos(\Omega t) = \cos(\Omega(T - t))$, that $\cos(\Omega t + \phi_0) = \cos(\Omega(T - t) - \phi_0)$, and that $\sigma^{x,z}$ are real whereas σ^y is imaginary, we define an operator

$$\mathcal{U}'_T = (\mathcal{U}_T^{-1})^* \quad (7)$$

$$= \mathfrak{T} e^{-i \int_0^T dt h'(k_x, k_y, A_{0x}, A_{0y}, \phi_0, t)}. \quad (8)$$

This means that \mathcal{U}'_T is the Floquet operator corresponding to a different time-dependent Hamiltonian $h'(k_x, k_y, A_{0x}, A_{0y}, \phi_0, t)$ which can be transformed back to $h(k_x, k_y, A_{0x}, A_{0y}, \phi_0, t)$ in one of two ways. We can keep ϕ_0 unchanged, interchange $k_x \leftrightarrow k_y$ and $A_{0x} \leftrightarrow A_{0y}$, shift time $t \rightarrow t + \phi_0/\Omega$ (this does not change the Floquet eigenvalues), and, finally, perform a rotation by $\pi/2$ about the z axis which transforms $\sigma^y \rightarrow -\sigma^x$ and $\sigma^x \rightarrow \sigma^y$. [Such a rotation which is independent of k_x, k_y unitarily transforms both the Floquet operator and its eigenstates but does not change the Chern number defined in Eq. (11) below.] Alternatively, we can change $\phi_0 \rightarrow \pi - \phi_0$ and $k_y \rightarrow -k_y$ but keep k_x, A_{0x} , and A_{0y} unchanged. From Eqs. (5) and (7), we see that

$$\mathcal{U}'_T \psi_\alpha^* = e^{-i\epsilon_\alpha T} \psi_\alpha^*. \quad (9)$$

Hence \mathcal{U}_T and \mathcal{U}'_T have the same quasienergies; in particular, the positive quasienergy band of \mathcal{U}_T is also the positive quasienergy band of \mathcal{U}'_T , and their eigenstates ψ_α and ψ'_α are related as

$$\psi'_\alpha = \psi_\alpha^*. \quad (10)$$

Finally, consider that the Chern number in the positive quasienergy band is

$$C_+(A_{0x}, A_{0y}, \phi_0) = \frac{i}{2\pi} \int d^2k \left[\frac{\partial \psi_\alpha^\dagger}{\partial k_x} \frac{\partial \psi_\alpha}{\partial k_y} - \frac{\partial \psi_\alpha^\dagger}{\partial k_y} \frac{\partial \psi_\alpha}{\partial k_x} \right]. \quad (11)$$

We now see that this does not change if we complex conjugate ψ [as dictated by Eq. (10)] and either interchange $k_x \leftrightarrow k_y$ or change $k_y \rightarrow -k_y$ but do not change k_x . The discussion above therefore shows that the Chern number $C_+(A_{0x}, A_{0y}, \phi_0)$ must remain the same if either we keep ϕ_0 unchanged and interchange $A_{0x} \leftrightarrow A_{0y}$ or we change $\phi_0 \rightarrow \pi - \phi_0$ but keep A_{0x} and A_{0y} unchanged. This explains the two symmetries which are visible in Fig. 2. (See Supplemental Material [40].)

Figure 2 shows that the Chern numbers are not opposite for ϕ and $-\phi$, even though the vector potentials for ϕ and $-\phi$ are time-reversal counterparts of each other [see Eq. (4)]. This is because the time-independent part of the Hamiltonian breaks time-reversal symmetry.

Floquet edge modes. In order to test the bulk-boundary correspondence for this driven system, we consider an infinitely long nanoribbon as we did in the equilibrium case and perturb it using polarized light described by a vector potential in Eq. (4). This introduces a time dependence into the Hamiltonian in Eq. (3), which we incorporate by minimal coupling and Peierls substitution, i.e., $k_x \rightarrow k_x + A_{0x} \cos(\Omega t)$, $\gamma \rightarrow \gamma e^{iA_{0y} \cos(\Omega t + \phi_0)}$, and $\Delta \rightarrow \Delta e^{iA_{0y} \cos(\Omega t + \phi_0)}$. We then diagonalize the Floquet operator constructed using this time-dependent Hamiltonian to obtain the quasienergies which are shown as a function of momentum k_x in Fig. 3.

While we have fixed $\phi_0 = -\pi/2$, the four panels of Fig. 3 correspond to four different pairs of drive amplitudes (A_{0x}, A_{0y}). All these lie in four different phases of Fig. 2(c). The continuum formed by the bulk states is shown in blue with the brighter colors denoting the primary Floquet zone, i.e., $\epsilon T = -\pi$ to π . The muted colors show parts of the secondary Floquet zones. These bands are separated by energy gaps which host the modes localized along the edges of the ribbon (green for the top edge and red for the bottom edge). Depending upon the ratio of A_{0x} and A_{0y} , edge modes exist at $\epsilon T = 0$ and/or $\epsilon T = \pi$. These edge states are also eigenstates of σ^x . The right-pointing (left-pointing) triangles correspond to states with $\sigma^x = 1$ ($\sigma^x = -1$), respectively. The insets are magnified views of the edge-state dispersion. In Fig. 3(a), we see that there are two kinds of edge states: one per edge at $\epsilon T = 0$ and two per edge at $\epsilon T = \pm\pi$. This lies in the $C_+ = -1$ phase of Fig. 2(c). On the other hand, Fig. 3(b) has only one set of edge states at $\epsilon T = 0$, which is consistent with the $C_+ = 1$ in this phase. Figure 3(c) depicts $C_+ = 0$ phase and therefore has no edge modes, while Fig. 3(d) lies in the $C_+ = -2$ phase and has two sets of edge modes, both close to $\epsilon T = \pm\pi$. From this we infer that a pair of edge states at $\epsilon = 0$ correspond to $C_+ = +1$, whereas each pair of states at $\epsilon T = \pm\pi$ corresponds to $C_+ = -1$. These add up along with the signs to give the total Chern number C_+ . We note that if we start with an equilibrium system in a different region of Fig. 1(a), we can access Floquet topological phases with Chern number $C_+ \in [-1, 2]$,

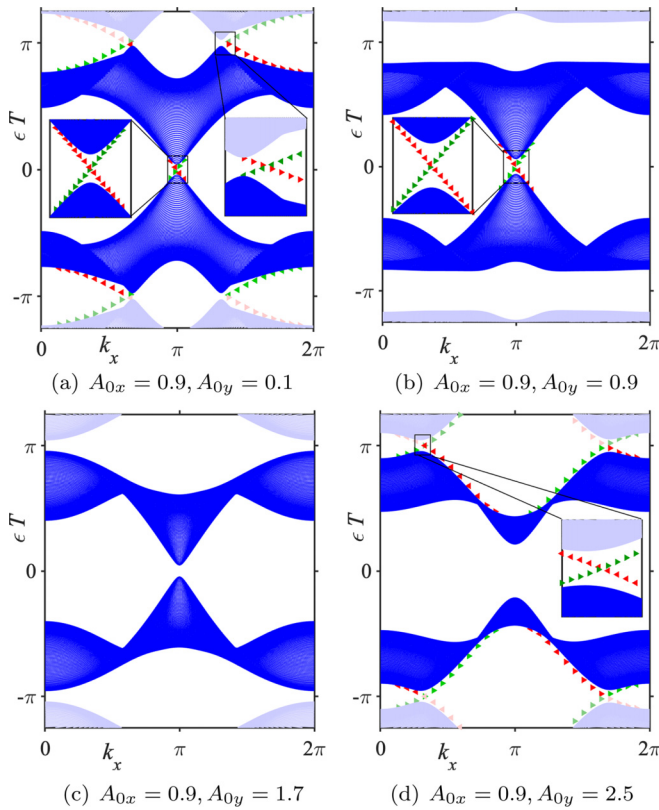


FIG. 3. Floquet edge modes on a ribbon along the \hat{x} direction with a width $N_y = 100$ along the \hat{y} direction, with a drive frequency $\Omega = 5$. These correspond to four different regions in the phase diagram shown in Fig. 2(c) for $\phi_0 = -\pi/2$ with Chern numbers $C_+ = -1, 1, 0,$ and -2 , respectively. The right-pointing (left-pointing) triangles depict states with spin pointing along the \hat{x} ($-\hat{x}$) directions, while the color red (green) corresponds to the bottom (top) edge of the nanoribbon. In all the panels, the bulk states are shown in blue. The primary Floquet zone is shown in brighter colors and ranges from $\epsilon T = -\pi$ to $\epsilon T = \pi$, while the muted colors show parts of the secondary Floquet zones. (b) corresponds to circular polarization, while (a), (c), and (d) correspond to a more general elliptically polarization.

Results and discussion. We discuss the effects of an optical drive in the form of a general elliptically polarized light on a half-BHZ system. A range of topological phases corresponding to different Chern numbers can be generated purely by varying the driving parameters, namely, the amplitudes of the vector potential in the \hat{x} and \hat{y} directions and their phase difference ϕ_0 . We interpret this as an effect of the anisotropy that elliptically polarized light introduces into the time-dependent Hamiltonian.

Fixing the phase $\phi_0 = \pi/2$ and varying only the ratio of A_{0x} and A_{0y} allow us to tune in and out of topological

phases even when we deviate away from the special case of circular polarization. The Chern numbers are consistent with the number of spin-polarized states localized at the two edges of an infinitely long nanoribbon with the edge states having a definite value of σ^x .

A striking feature of the Floquet phase diagram is the existence of multicritical points. This feature can be seen only when one is away from the special cases of both linear and circular polarization. At this point, four phases with distinct Chern numbers intersect.

While the equilibrium model has phases with Chern numbers $0, \pm 1$, the time-dependent system driven out of equilibrium using an elliptically polarized light allows us to generate Floquet topological phases with higher Chern numbers as shown in Fig. 2. Similarly, choosing the drive parameters appropriately, the topology can even be destroyed using such an optical drive. Thus elliptically polarized light allows us to engineer and/or modify topological phases in the half-BHZ system.

As is well known, a BHZ-type system can be realized in an HgTe/CdTe quantum well with a band gap $\Delta E \approx 0.3$ eV and a lattice constant $a \approx 0.5$ nm. All our parameters are defined in units of ΔE and a . Choosing the parameters appropriately, we can realize the desired Floquet topological phase. For instance, if we choose $A_{0x,y} \approx (0.3, 1.2)$ and $\phi_0 = -\pi/2$, we would be close to a multicritical point in Fig. 2(c). The time scale of observation should be large compared with the time period T so that the concept of a Floquet Hamiltonian is valid. Another possible realization is in the context of topological bound states of photonic systems where a lattice of coupled optical waveguides is used to emulate the behavior of time-dependent condensed matter systems [43].

We have confined our discussion to the case of two-dimensional topological insulators with one-dimensional edge modes. However, the effect of elliptical polarization could have more significance in the context of higher-order topological systems [44]. For instance, since generating a two-dimensional second-order TI with corner modes requires a perturbation that breaks the C_4 symmetry, one can expect that using elliptically polarized light (away from the special case of circular polarization) could also achieve the same [45], since the incident light (and hence the effective Floquet Hamiltonian) breaks the fourfold rotation symmetry. We note, however, that a two-dimensional higher-order topological system requires a model with at least four bands, while we have only considered a two-band model here.

Acknowledgments. R.S. thanks Devendra Singh Bhakuni and Anurag Banerjee for useful discussions. R.S. and D.S. thank Seabrata Mukherjee for useful discussions. D.S. thanks SERB, India, for funding through Project No. JBR/2020/000043.

- [1] M. Z. Hasan and C. L. Kane, Colloquium: Topological insulators, *Rev. Mod. Phys.* **82**, 3045 (2010).
- [2] B. A. Bernevig, T. L. Hughes, and S.-C. Zhang, Quantum spin Hall effect and topological phase transition in HgTe quantum wells, *Science* **314**, 1757 (2006).

- [3] J. E. Moore, The birth of topological insulators, *Nature (London)* **464**, 194 (2010).
- [4] J. E. Moore and L. Balents, Topological invariants of time-reversal-invariant band structures, *Phys. Rev. B* **75**, 121306(R) (2007).

- [5] L. Fu, C. L. Kane, and E. J. Mele, Topological Insulators in Three Dimensions, *Phys. Rev. Lett.* **98**, 106803 (2007).
- [6] R. Seshadri, K. Sengupta, and D. Sen, Edge states, spin transport, and impurity-induced local density of states in spin-orbit coupled graphene, *Phys. Rev. B* **93**, 035431 (2016).
- [7] T. Kitagawa, E. Berg, M. Rudner, and E. Demler, Topological characterization of periodically driven quantum systems, *Phys. Rev. B* **82**, 235114 (2010).
- [8] T. Kitagawa, T. Oka, A. Brataas, L. Fu, and E. Demler, Transport properties of nonequilibrium systems under the application of light: Photoinduced quantum Hall insulators without Landau levels, *Phys. Rev. B* **84**, 235108 (2011).
- [9] T. Oka and H. Aoki, Photovoltaic Hall effect in graphene, *Phys. Rev. B* **79**, 081406(R) (2009).
- [10] Z. Gu, H. A. Fertig, D. P. Arovas, and A. Auerbach, Floquet Spectrum and Transport through an Irradiated Graphene Ribbon, *Phys. Rev. Lett.* **107**, 216601 (2011).
- [11] N. H. Lindner, G. Refael, and V. Galitski, Floquet topological insulator in semiconductor quantum wells, *Nat. Phys.* **7**, 490 (2011).
- [12] E. Suárez Morell and L. E. F. Foa Torres, Radiation effects on the electronic properties of bilayer graphene, *Phys. Rev. B* **86**, 125449 (2012).
- [13] A. Kundu, H. A. Fertig, and B. Seradjeh, Effective Theory of Floquet Topological Transitions, *Phys. Rev. Lett.* **113**, 236803 (2014).
- [14] B. Dóra, J. Cayssol, F. Simon, and R. Moessner, Optically Engineering the Topological Properties of a Spin Hall Insulator, *Phys. Rev. Lett.* **108**, 056602 (2012).
- [15] M. Thakurathi, A. A. Patel, D. Sen, and A. Dutta, Floquet generation of Majorana end modes and topological invariants, *Phys. Rev. B* **88**, 155133 (2013).
- [16] Y. T. Katan and D. Podolsky, Modulated Floquet Topological Insulators, *Phys. Rev. Lett.* **110**, 016802 (2013).
- [17] H.-X. Zhu, T.-T. Wang, J.-S. Gao, S. Li, Y.-J. Sun, and G.-L. Liu, Floquet topological insulator in the BHZ model with the polarized optical field, *Chin. Phys. Lett.* **31**, 030503 (2014).
- [18] M. S. Rudner, N. H. Lindner, E. Berg, and M. Levin, Anomalous Edge States and the Bulk-Edge Correspondence for Periodically Driven Two-Dimensional Systems, *Phys. Rev. X* **3**, 031005 (2013).
- [19] F. Nathan and M. S. Rudner, Topological singularities and the general classification of Floquet–Bloch systems, *New J. Phys.* **17**, 125014 (2015).
- [20] D. Carpentier, P. Delplace, M. Fruchart, and K. Gawędzki, Topological Index for Periodically Driven Time-Reversal Invariant 2D Systems, *Phys. Rev. Lett.* **114**, 106806 (2015).
- [21] T.-S. Xiong, J. Gong, and J.-H. An, Towards large-Chern-number topological phases by periodic quenching, *Phys. Rev. B* **93**, 184306 (2016).
- [22] M. Thakurathi, D. Loss, and J. Klinovaja, Floquet Majorana fermions and parafermions in driven Rashba nanowires, *Phys. Rev. B* **95**, 155407 (2017).
- [23] B. Mukherjee, P. Mohan, D. Sen, and K. Sengupta, Low-frequency phase diagram of irradiated graphene and a periodically driven spin- $\frac{1}{2}$ XY chain, *Phys. Rev. B* **97**, 205415 (2018).
- [24] L. Zhou and J. Gong, Recipe for creating an arbitrary number of Floquet chiral edge states, *Phys. Rev. B* **97**, 245430 (2018).
- [25] Q. Chen, L. Du, and G. A. Fiete, Floquet band structure of a semi-Dirac system, *Phys. Rev. B* **97**, 035422 (2018).
- [26] C. Dutreix, E. A. Stepanov, and M. I. Katsnelson, Laser-induced topological transitions in phosphorene with inversion symmetry, *Phys. Rev. B* **93**, 241404(R) (2016).
- [27] P. M. Perez-Piskunow, G. Usaj, C. A. Balseiro, and L. E. F. Foa Torres, Floquet chiral edge states in graphene, *Phys. Rev. B* **89**, 121401(R) (2014).
- [28] J. W. McIver, B. Schulte, F.-U. Stein, T. Matsuyama, G. Jotzu, G. Meier, and A. Cavalleri, Light-induced anomalous Hall effect in graphene, *Nat. Phys.* **16**, 38 (2020).
- [29] T. Nag, R.-J. Slager, T. Higuchi, and T. Oka, Dynamical synchronization transition in interacting electron systems, *Phys. Rev. B* **100**, 134301 (2019).
- [30] T. V. Trevisan, P. V. Arribi, O. Heinonen, R.-J. Slager, and P. P. Orth, Bicircular Light Floquet Engineering of Magnetic Symmetry and Topology and Its Application to the Dirac Semimetal Cd₃As₂, *Phys. Rev. Lett.* **128**, 066602 (2022).
- [31] P. Delplace, A. Gómez-León, and G. Platero, Merging of Dirac points and Floquet topological transitions in ac-driven graphene, *Phys. Rev. B* **88**, 245422 (2013).
- [32] A. Gómez-León, P. Delplace, and G. Platero, Engineering anomalous quantum Hall plateaus and antichiral states with ac fields, *Phys. Rev. B* **89**, 205408 (2014).
- [33] K. Takasan, M. Nakagawa, and N. Kawakami, Laser-induced phase transitions of topological Kondo insulators, *Phys. Procedia* **75**, 447 (2015).
- [34] K. Kitayama, Y. Tanaka, M. Ogata, and M. Mochizuki, Floquet theory of photoinduced topological phase transitions in the organic salt α -(BEDT-TTF)₂I₃ irradiated with elliptically polarized light, *J. Phys. Soc. Jpn.* **90**, 104705 (2021).
- [35] D. Baykusheva, A. Chacón, J. Lu, T. P. Bailey, J. A. Sobota, H. Soifer, P. S. Kirchmann, C. Rotundu, C. Uher, T. F. Heinz, D. A. Reis, and S. Ghimire, All-optical probe of three-dimensional topological insulators based on high-harmonic generation by circularly polarized laser fields, *Nano Lett.* **21**, 8970 (2021).
- [36] H. Chnafa, M. Mekkaoui, A. Jellal, and A. Bahaoui, Effect of strain on band engineering in gapped graphene, *Eur. Phys. J. B* **94**, 39 (2021).
- [37] A. Díaz-Fernández, Inducing anisotropies in Dirac fermions by periodic driving, *J. Phys.: Condens. Matter* **32**, 495501 (2020).
- [38] A. Altland and M. R. Zirnbauer, Nonstandard symmetry classes in mesoscopic normal-superconducting hybrid structures, *Phys. Rev. B* **55**, 1142 (1997).
- [39] T. Fukui, Y. Hatsugai, and H. Suzuki, Chern numbers in discretized Brillouin zone: Efficient method of computing (spin) Hall conductances, *J. Phys. Soc. Jpn.* **74**, 1674 (2005).
- [40] See Supplemental Material at <http://link.aps.org/supplemental/10.1103/PhysRevB.106.245401> for details.
- [41] G. Floquet, On linear differential equations with periodic coefficients, *Sci. Ann. Ec. Norm. Super. 2nd Ser.* **12**, 47 (1883).
- [42] M. Holthaus, Floquet engineering with quasienergy bands of periodically driven optical lattices, *J. Phys. B: At. Mol. Opt. Phys.* **49**, 013001 (2016).
- [43] S. Mukherjee, A. Spracklen, M. Valiente, E. Andersson, P. Öhberg, N. Goldman, and R. R. Thomson, Experimental observation of anomalous topological edge modes in a slowly driven photonic lattice, *Nat. Commun.* **8**, 13918 (2017).

- [44] R. Seshadri, A. Dutta, and D. Sen, Generating a second-order topological insulator with multiple corner states by periodic driving, *Phys. Rev. B* **100**, 115403 (2019).
- [45] Z. Ning, B. Fu, D.-H. Xu, and R. Wang, Tailoring quadrupole topological insulators with periodic driving and disorder, *Phys. Rev. B* **105**, L201114 (2022).